Modeling multi-modal traffic in cities

Conference Paper

Author(s):
Loder, Allister; Bressan, Lea; Ambühl, Lukas; Bliemer, Michiel C.J.; Axhausen, Kay W.

Publication date:
2018-05

Permanent link:
https://doi.org/10.3929/ethz-b-000264726

Modeling multi-modal traffic in cities

Allister Loder

Lea Bressan

Lukas Ambühl

Michiel C.J. Bliemer

Monica Menendez

Kay W. Axhausen

Institute for Transport Planning and Systems

May 2018

STRC

18th Swiss Transport Research Conference

Monte Verità / Ascona, May 16 – 18, 2018

Institute for Transport Planning and Systems

Modeling multi-modal traffic in cities

Allister Loder, Lukas Ambühl
IVT
ETH Zürich

CH-8093 Zürich
phone: +41 44 633 62 58
fax: +41 44 633 10 57

Lea Bressan

ETH Zürich

CH-8093 Zürich
phone:
fax: +41 44 633 10 57
bressanl@student.ethz.ch

Michiel C.J. Bliemer
Institute of Transport and Logistics Studies
University of Sydney

NSW 2006, Australia
phone: +61 2 9114 1840
fax: +61 2 9114 1863
michiel.bliemer@sydney.edu.au

{allister.loder,lukas.ambuehl}@ivt.baug.ethz.ch

Monica Menendez
Division of Civil Engineering
NYU Abu Dhabi

phone: +971-2-628-5273

monica.menendez@nyu.edu

Kay W. Axhausen
IVT
ETH Zürich

CH 8093 Zürich, Switzerland
phone: +41 44 633 39 43
fax: +41 44 633 10 57
axhausen@ivt.baug.ethz.ch

May 2018

Abstract

We propose a new functional form for the 3D-MFD. The 3D-MFD links the number of cars and buses in an urban network to the total travel production. The parameters of the functional form are derived from the structure and topology of the road and bus network. The physical interactions of vehicles are described by a single parameter. We apply the methodology to two empirical data sets from London and Zurich, and discuss policy relevant applications of the functional form.

Keywords

Keywords, in English

1 Introduction

Cities are complex and so are their transportation systems. As all modes of transportation compete for scarce urban resources such as space and funding, their interactions determine the optimum allocation of urban resources to achieve optimal productivity of the entire system. In terms of road traffic, one of the most recognizable interactions is between cars and buses (trams) on urban roads. There exist many images and studies that summarize the trade-off between the cruising speed and space consumption of the two modes and that raise the question of the optimal share between them. Smeed (1968) was among the first to discuss this issue analytically, but methods beyond a simple bus-car-equivalent for entire cities did not exist before the concept of the three-dimensional macroscopic fundamental diagram (3D-MFD) was introduced (Geroliminis et al., 2014).

The 3D-MFD captures many (joint) effects of bus and car externalities on the total production of travel, either from a vehicle or passenger perspective. 3D-MFDs are either estimated with simulation or empirical observations (Geroliminis et al., 2014; Loder et al., 2017; Castrillon and Laval, 2017) or derived analytically in conceptual contexts (Chiabaut, 2015; Boyaci and Geroliminis, 2011). So far, no functional form for the 3D-MFD exists and no proposal has been made that links physical properties of road and bus network topology and operations to the shape of the 3D-MFD. Such a perspective would facilitate the analysis of the productivity of entire multi-modal urban networks as the theory of the macroscopic fundamental diagram (MFD) already does for cars (Daganzo, 2007). In this paper, however, we propose a functional form for the 3D-MFD with parameters solely derived from the properties of the networks and multi-modal traffic operations.

This functional form for the 3D-MFD is defined by creating a three-dimensional lower envelope of planes where the parameters reflect physical characteristics of the network and traffic operations. The parameters of the planes reflect the influence of traffic signals (Daganzo et al., 2017; Daganzo and Lehe, 2016; Daganzo and Geroliminis, 2008) and bus operations (Boyaci and Geroliminis, 2011; Guler and Menendez, 2014) on the system's capacity. The resulting three-dimensional lower envelope describes the upper 3D-MFD that bounds all possible traffic states (Daganzo and Geroliminis, 2008; Daganzo and Lehe, 2016). Then, we obtain a strictly concave and smooth functional form by using the smooth approximation of the minimum operator (Ambühl et al., 2017), where a single smoothing parameter quantifies interactions between vehicles that reduce travel production. The proposed method shares ideas with the method of cuts for the MFD estimation (Daganzo and Geroliminis, 2008; Leclercq and Geroliminis, 2013) and our approach is flexible to accommodate any derived three-dimensional cuts or any other parametrization of physical boundaries in urban traffic systems.

This paper is organized as follows. Section 2 introduces the new functional form, discusses the parameters and how the lower envelope of the 3D-MFD is built based on the network and operational parameters. We then show how this functional form can be used in applications in Section 3, before applying the proposed functional form to two empirical data sets from London (UK) and Zurich (CH) in Section 4.

2 A new functional form

This functional relationships extends the approach by Ambühl et al. (2017) for car traffic to the multi-modal case of the 3D-MFD by defining three-dimensional planes instead of two-dimensional lines. In the approach for car traffic only, the lower envelope or upper MFD between flow q and density k can be represented by Eqn. 1 with a trapezoidal shape (Daganzo et al., 2017; Ambühl et al., 2017) with parameters free flow speed v, capacity Q, wave speed w and jam density κ that bounds flow for any level of vehicle density. In the following, we show how to apply this idea to the 3D-MFD.

$$q\left(k\right) = \min\left(vk; Q; w\left(\kappa - k\right)\right) \tag{1}$$

2.1 Elementary equation

Conventionally in the 3D-MFD, the accumulation of cars N_c and buses N_b is related to the total travel production Π of vehicles or passengers (Geroliminis et al., 2014; Loder et al., 2017). The accumulations are in vehicles and the production is in vehicle or passenger kilometer per hour. When applying in Sections 3 and 4 the proposed functional form, we use vehicle densities instead of accumulations, in units of vehicles per lane-meter, and vehicle-kilometer per second instead of hour to achieve manageable numbers. To adopt Eqn. 1 for the 3D-MFD, we create a three dimensional lower envelope consisting of J planes that provide an upper limit for the travel production for a given combination of accumulations of both modes. We will discuss a certain set of planes in Section 2.3, but J must be specified for each city context. We define plane i in the N_c, N_b and Π space as given in Eqn. 2 with a point on the plane with coordinates

$(car_{0,i}, bus_{0,i}, \pi_{0,i})$ and a normal vector with coordinates $(car_{n,i}, bus_{n,i}, \pi_{n,i})$.

$$\left(\begin{pmatrix} N_c \\ N_b \\ \Pi \end{pmatrix} - \begin{pmatrix} car_{0,i} \\ bus_{0,i} \\ \pi_{0,i} \end{pmatrix}\right)^T \cdot \begin{pmatrix} car_{n,i} \\ bus_{n,i} \\ \pi_{n,i} \end{pmatrix} = 0 \tag{2}$$

After solving Eqn. 2 for Π we obtain Eqn. 3 for plane Π_i as a function of both modes' vehicle accumulations.

$$\Pi_i\left(N_c, N_b\right) = \pi_{0,i} - \left(car_{n,i}\left(N_c - car_{0,i}\right) + bus_{n,i}\left(N_b - bus_{0,i}\right)\right)/\pi_{n,i} \tag{3}$$

The 3D-MFD with $\Pi_i\left(N_c, N_b\right)$ is then defined as the minimum travel production of the J planes for a combination of N_c and N_b as shown in Eqn. 4; similar to the idea of cuts by Daganzo and Geroliminis (2008) and the trapezoidal lower envelope in Eqn. 1.

$$\Pi\left(N_c, N_b\right) = \min\left(\Pi_1; \Pi_2; \Pi_3; \ldots; \Pi_J\right) \tag{4}$$

We then apply the smooth approximation of the minimum operator (Ambühl et al., 2017) to Eqn. 4 and obtain a strictly concave relationship as shown in Eqn. 5.

$$\Pi\left(N_c, N_b\right) = -\lambda \log\left(\exp\left(-\frac{\Pi_1}{\lambda}\right) + \exp\left(-\frac{\Pi_2}{\lambda}\right) + \exp\left(-\frac{\Pi_3}{\lambda}\right) + \cdots + \exp\left(-\frac{\Pi_J}{\lambda}\right)\right) \tag{5}$$

In Eqn. 5, the parameter λ describes the smoothing of the function to the three-dimensional lower envelope defined by the J plane. The closer λ is to zero, the more the function aligns to the three-dimensional lower envelope.

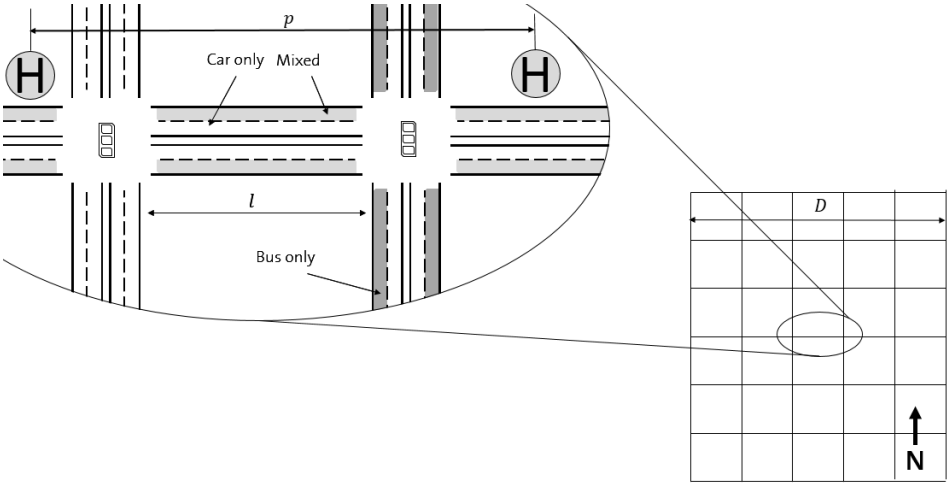

Figure 1: Abstract network for illustrating the most relevant parameters of multi-modal urban road networks.

2.2 The λ parameter

The most important parameter of Eqn. 5 is the smoothing parameter λ because of its interpretation in the 3D-MFD context. λ quantifies with a single parameter the losses in travel production due to vehicle interactions in the network. It is clear from the definition of Eqn. 5 that this parameter is highly non-linear, but provides an opportunity to reduce complexity to a single value. If $\lambda = 0$, no vehicle level interactions take place and the larger the value becomes the stronger the total production is reduced by interactions and mixing of traffic.

A procedure to obtain a suitable value for λ in a network is to estimate λ from observations, e.g. empirical or simulation data. However, future research has to explore whether λ can be derived analytically or predicted with a model estimated from empirical observations.

2.3 Defining the three-dimensional lower envelope

In this section, we consider an abstract grid network as exhibited in Figure 1. Intersections are spaced regularly at a distance l and the side length of the entire network is approximated by D. The entire network length in lane-kilometer is L. We distinguish three different types of lanes: Dedicated car lanes, dedicated bus lanes and mixed lanes. Here, we consider η_b and η_c the fraction of the network length where only buses and cars circulate, respectively. Thus, the total network length where only cars circulate is $\eta_c L$, where only buses circulate $\eta_b L$ and where both circulate is $(1 - \eta_b - \eta_c)L$. The bus stops are spaced regularly with a distance p. The headway of buses then follows from the design of the network and the number of buses Daganzo (2010).

Name	Key	Unit	Additional comments
Variables			
Accumulation of cars	N_c	[veh]	Normalized to density by dividing with the car network length.
Accumulation of buses	N_b	[veh]	Normalized to density by dividing with the bus network length.
Total travel production	Π	[veh-km/h]	
Average speed in the network	v_{MFD}	[km/h]	
Speed of cars in the network	$v_{c,MFD}$	[km/h]	
Speed of buses in the network	$v_{b,MFD}$	[km/h]	
Parameters			
Smoothing parameter	λ	[-]	Value is shape specific.
Total network length	L	[km]	Entire urban road infrastructure.
Fraction of car only roads	η_c	[-]	
Fraction of bus only roads	η_b	[-]	
Jam spacing of cars	l_c	[km]	
Passenger car equivalent of buses	φ	[-]	
Average car delay at intersections	δ_c	[h]	
Free-flow speed of cars	$v_{c,0}$	[km/h]	
Backward wave speed of cars	$w_{c,0}$	[km/h]	
Free-flow speed of buses	$v_{b,0}$	[km/h]	
Backward wave speed of buses	$w_{b,0}$	[km/h]	
Saturation flow of cars	s_c	[veh/h-lane]	
Saturation flow of buses	s_b	[veh/h-lane]	Computed from the bus fundamental diagram.
Intersection spacing	l	[km]	
Stop spacing	p	[km]	
Dwell time	Δ	[s]	
Cycle length	C	[s]	
Effective green time	G	[s]	
Public transport strategy	ζ	[-]	If 0, buses have ultimate priority at signals. If 1, buses are entirely mixed with cars and experience the same delay.

Table 1: 3D-MFD variables in the upper part and input parameters for the lower envelope for the 3D-MFD. Further parameters calculated from these input parameters are not shown for convenience.

Table 1 summarizes all variables and parameters used in the following. No real city will ever match this abstract grid network, but as we aim at a macroscopic perspective of multi-modal urban traffic, network-wide averages of any network topology will provide important insights to the multi-modal trade-offs.

The planes for Eqn. 5 will be defined from thirteen points that we introduce in the following. Figure 7 shows the location of all points in the 3D-MFD. Here, we focus primarily on planes defining a lower envelope for geometric reasons, but also discuss one operational feature of multi-modal traffic. Additional operational features can be included if necessary. All planes are defined by at least three points in the 3D-MFD, which are given in the Cartesian coordinate system in the order of N_c, N_b and Π. All resulting planes are summarized in Table 2.

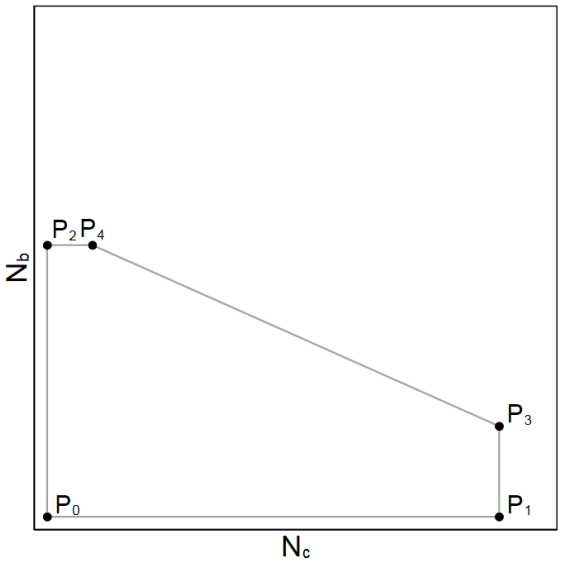

Figure 2: Top-down view on the 3D-MFD which shows the bimodal vehicle accumulation plane. The lines connecting the points represent a possible lower envelope for traffic states.

2.4 Defining the points

The trivial point in the system is point $P_0 = (0, 0, 0)^T$ at the origin where no vehicles in the network circulate and thus do not produce any kilometers. Consider then the top down view on the car and bus accumulation plane in Figure 2. Cars can drive on $(1 - \eta_b)\, L$ of the network and have a jam spacing l_c. The point P_1 is the maximum accumulation in the network of cars possible when no public transport operates and the network is gridlocked. The point then equals

$$P_1 = \begin{pmatrix} (1 - \eta_b)\, L/l_c \\ 0 \\ 0 \end{pmatrix}$$

The point P_2 considers the case when no cars circulate and the bus system is gridlocked on $(1 - \eta_c)\, L$ of the network. For the buses, we make the assumption that the passenger car equivalent is φ. Then the point is defined by

$$P_2 = \begin{pmatrix} 0 \\ (1 - \eta_c)\, L/\,(l_c \varphi) \\ 0 \end{pmatrix}$$

Next, we define the gridlock boundary under mixed traffic conditions with the points P_3 and P_4 where the production of traffic is zero. The point P_3 describes gridlock for all car and mixed

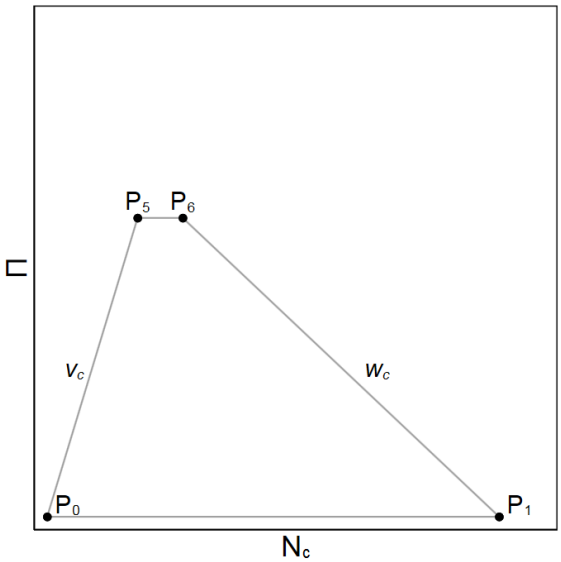

Figure 3: Side view on the 3D-MFD on the total travel production and car accumulation plane. For the defined points, no public transport operates.

lanes as well as gridlock on all dedicated bus lanes and equals

$$P_3 = \begin{pmatrix} (1-\eta_b)\, L/l_c \\ \eta_b L/\left(l_c \varphi\right) \\ 0 \end{pmatrix}$$

while the point P_4 mirrors this behavior for buses and is defined with

$$P_4 = \begin{pmatrix} \eta_c L/l_c \\ (1-\eta_c)\, L/\left(l_c \varphi\right) \\ 0 \end{pmatrix}$$

Then, we only consider the situation where no public transport operates, i.e. $N_b = 0$. At intersections, cars experience on average a delay of δ_c that reduce the street free-flow speed $v_{c,0}$ at the network level to v_c. We approximate the network-wide average free-flow speed v_c as simple as possible by Eqn. 6, but more sophisticated approaches could also be used, e.g. by Daganzo and Geroliminis (2008). The network-wide average backward wave speed for cars w_c is obtained in a similar way as given in Eqn. 6, where the street backward wave speed $w_{c,0}$

replaces the free flow speed $v_{c,0}$.

$$v_c = \frac{l}{\frac{l}{v_{c,0}} + \delta_c} \tag{6}$$

Figure 3 shows the discussed situation with $N_b = 0$ and the network-wide speeds v_c and w_c, which is basically the MFD as defined in Eqn. 1. The points P_0 and P_1 are already defined and only points P_5 and P_6 must be defined. Both points share the common total travel production given by Eqn. 7.

$$\Pi_c = s_c L \left(1 - \eta_b\right) \frac{G}{C} \tag{7}$$

Equation 7 is derived from the stationary cut defined by Daganzo and Geroliminis (2008) with the saturation flow s_c, the cycle length C and the effective green time G. We derive N_c for both points with the fundamental relationship of traffic using the free flow speed v_c and backward wave speed w_c as shown in Figure 3. Then, points P_5 and P_6 equal to

$$P_5 = \begin{pmatrix} \Pi_c / v_c \\ 0 \\ \Pi_c \end{pmatrix}$$

$$P_6 = \begin{pmatrix} \left(1 - \eta_b\right) \frac{L}{l_c} - \Pi_c / w_c \\ 0 \\ \Pi_c \end{pmatrix}$$

We then follow the same argumentation for the case with only buses operating and no cars circulating, i.e. $N_c = 0$. Figure 4 exhibits this situation where the points P_0 and P_2 are already defined. Thus, we define points P_7 and P_8 similarly to P_5 and P_6. However, buses have to stop not only at intersections but also at bus stops for boarding and alighting of passengers during the dwell time period Δ. For simplicity, we assume that the dwell time also includes deceleration

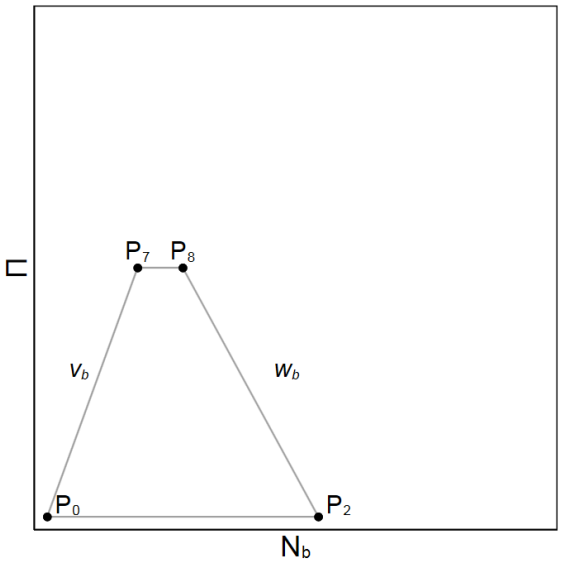

Figure 4: Side view on the 3D-MFD with the total travel production versus the accumulation of buses. No cars are operating.

and acceleration and that the public transport operator has defined for each stop a scheduled arrival and departure time so that Δ is under normal circumstances independent of the demand and human behavior.

Some public transport agencies wish to include a buffer in the travel time between two stops that allows an operation within a rigid time table even under more congested traffic situations. So, buses would be equipped with a device that gives drivers advice about the scheduled travel time and that tells them to drive faster or slower, e.g. as implemented in Zurich's bus and tram system. As a consequence, buses would drive at a lower maximum speed $v_{b,0}$ then cars with $v_{c,0}$ in light traffic. Bus stops are placed at distance p. Some cities, e.g. Zurich, decided to give public transport full priority at each intersection to minimize delay for public transport vehicles, but other cities do not make a difference between cars and public transport vehicles so that public transport vehicles experience the same delay as cars. To capture this strategy we define the public transport strategy parameter ζ in $0 \leq \zeta \leq 1$. The value zero means full public transport priority and one signifies buses fully integrated in traffic, i.e. including all car delays. Thus, the maximum commercial speed of buses v_b that includes dwelling, intersections delay and time table buffer is given by Eqn. 8. The bus backward wave speed w_b is then obtained by incorporating delays similar to Eqn. 8.

$$v_b = \frac{p}{\Delta + \frac{p}{v_{b,0}} + \delta_c \zeta \frac{p}{l}} \tag{8}$$

We assume that the maximum travel production of buses Π_b is achieved for the case of full public transport priority ($\zeta = 0$) with no delay at intersections. Π_b will be lower in case of similar delays at intersections for buses and cars ($\zeta = 1$). Eqn. 9 states Π_b similar to Π_c in Eqn. 7 for car traffic, but also accounts for the dwelling at stops and public transport strategy. The term $s_b L\,(1 - \eta_c)$ quantifies the possible maximum production in case of no delays or bus stops are considered. The remaining part of Eqn. 9 quantifies then the fraction of this possible maximum production than can be realized when delays and stopping behavior is accounted for. This idea is inspired by the stationary cut by Daganzo and Geroliminis (2008). This fraction considers the fraction of time buses are moving during. Here, we multiply the fraction for stopping for passengers and for stopping at signals to obtain a robust estimate of the maximum travel production.

$$\Pi_b = s_b L\,(1 - \eta_c)\left(\left(\frac{\frac{p}{v_{b,0}}}{\frac{p}{v_{b,0}} + \Delta}\right)\left(1 + \left(\frac{G}{C} - 1\right)\zeta\right)\right) \tag{9}$$

Consequently, points P_7 and P_8 are then defined by

$$P_7 = \begin{pmatrix} 0 \\ \Pi_b / v_b \\ \Pi_b \end{pmatrix}$$

$$P_8 = \begin{pmatrix} 0 \\ (1 - \eta_c)\,L/\,(l\varphi) - \Pi_b / w_b \\ \Pi_b \end{pmatrix}$$

We then define two additional points P_9 and P_{10}. They describe the influence of dedicated bus lanes on the multi-modal capacity of the network. Consider the case with buses running on dedicated lanes: Car traffic is not obstructed by buses and when more buses are added to the system, the travel production is increased at the same level of car accumulation. As we are interested in this framework to provide an upper bound for bi-modal traffic, the highest travel production is achieved when all dedicated bus lanes operate at capacity and the remaining network is filled with cars to capacity.

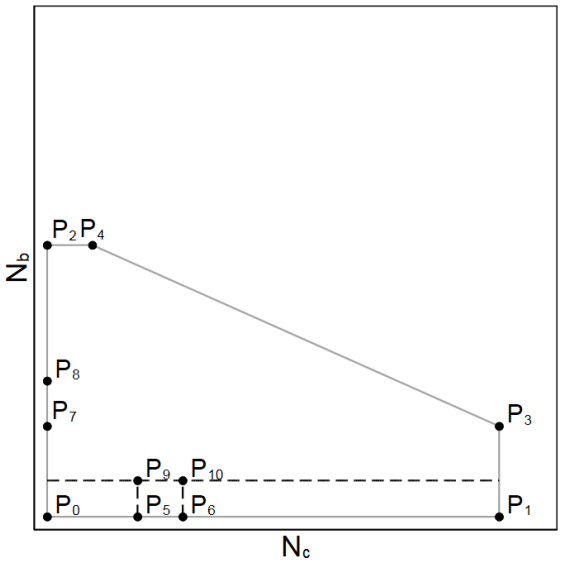

Figure 5: Additional points for the capacity in the 3D-MFD when buses on their dedicated lanes increase travel production from saturated car traffic.

Thus, the points P_9 and P_{10} are at the same car accumulation as P_5 and P_6 and at a public transport accumulation where capacity is reached on the dedicated bus lanes only. The latter sounds rather unrealistic when buses only use their dedicated lanes and not the mixed lanes as they usually run on fixed routes. Nevertheless, as we are interested in finding the lower envelope to the 3D-MFD, the highest possible production of bus kilometers for that amount of buses is only possible when all run on the dedicated network. Points P_9 and P_{10} are then defined as

$$P_9 = \begin{pmatrix} \Pi_c / v_c \\ \Pi_b \dfrac{\eta_b}{1-\eta_c} / v_b \\ \Pi_b \dfrac{\eta_b}{1-\eta_c} + \Pi_c \end{pmatrix}$$

$$P_{10} = \begin{pmatrix} (1-\eta_b)\dfrac{L}{l_c} - \Pi_c / w_c \\ \Pi_b \dfrac{\eta_b}{1-\eta_c} / v_b \\ \Pi_b \dfrac{\eta_b}{1-\eta_c} + \Pi_c \end{pmatrix}$$

The previously discussed set of points describes the physical limits of the system from a geometric perspective, from which we derive the lower envelope for the 3D-MFD or upper

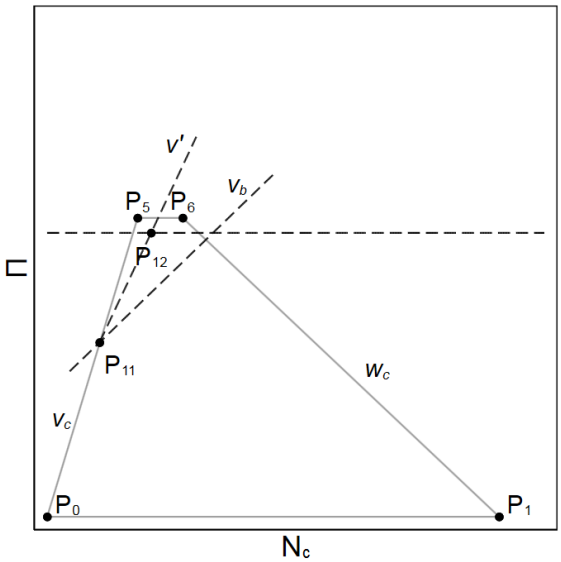

Figure 6: Including effects of mixed traffic in the 3D-MFD. The perspective shows the situation when few buses run on mixed lanes and thus slowing down cars.

bound for the 3D-MFD. However, there are many operational features in multi-modal networks that limit the productivity of networks further. These operational aspects can describe conflicts and effects in mixed traffic, bus bunching, dwelling behavior, effects of the built environment, e.g. bus stop design (curb side or bus bay), public transport network design and routing in the network.

We consider that most of these operational aspects result in context specific points and planes. Therefore, we focus here on one example of mixed traffic to illustrate the procedure. In cities, buses typically share road space with cars, but only drive on one lane in case the street has several lanes per direction. So one lane would be mixed and the other one dedicated to cars, see Figure 1. Arguably, most car drivers will first prefer to use their dedicated lanes before entering the mixed lanes, where they are slowed down by buses. In spatially heterogeneous networks, however, the mixing will be of course more complex that assumed here.

Figure 6 shows the influence of buses in mixed traffic for the horizontal arterial in Figure 1 (Nagai et al., 2005; Castrillon and Laval, 2017; Eichler and Daganzo, 2006). Note that Figure 6 shows P_0, P_1, P_5 and P_6 for orientation purposes, but the bus accumulation is just as such that it slows down cars in the mixed lanes. There is one lane only for cars and one mixed lane per driving direction. On this arterial, cars drive with speed v_c and buses with v_b, where buses are slower than cars. We assume that cars first drive on their dedicated lane as it is faster and switch to the mixed lane at speed v_b once the car only lane is saturated. The point at which capacity of the car only lane is reached is P_{11}. Once the mixed lane is operating at capacity the system reaches point P_{12} where capacity is reduced and the critical accumulation is increased.

The accumulation of cars where the moving bottleneck of buses is activated once all car only lanes are operating at capacity, i.e. $N_c = L\eta_c s\frac{G}{C}/v_c$ with a corresponding production of travel of $\Pi = L\eta_c s\frac{G}{C}$. After this accumulation of cars, any additional cars will drive at v_b, resulting in an average speed v' as defined by Eqn. 10.

$$v'(N_c) = \frac{L\eta_c s\frac{G}{C} + v_b\left(N_c - L\eta_c s\frac{G}{C}/v_c\right)}{N_c} \tag{10}$$

For defining the P_{11} and P_{12} we, we believe that it is context specific whether the bus accumulation and its contribution to production is set to zero for both points or to the values of P_9 and P_{10}. In case a non-zero contribution of buses is chosen, P_{11} and P_{12} evaluate to

$$P_{11} = \begin{pmatrix} L\eta_c s\frac{G}{C}/v_c \\ \Pi_b\frac{\eta_b}{1-\eta_c}/v_b \\ L\eta_c s\frac{G}{C} + \Pi_b\frac{\eta_b}{1-\eta_c} \end{pmatrix}$$

$$P_{12} = \begin{pmatrix} L\eta_b s\frac{G}{C}/v' \\ \Pi_b\frac{\eta_b}{1-\eta_c}/v_b \\ \Pi_b\frac{\eta_b}{1-\eta_c} + \varphi s_{bus}L\left(1-\eta_b-\eta_c\right)\frac{G}{C} + sL\left(1-\eta_b\right)\frac{G}{C} \end{pmatrix}$$

2.4.1 Defining the planes

Based on these thirteen points, we now propose a lower envelope for the 3D-MFD defined by a set of seven planes or nine planes if one wants to include the operational features discussed by points P_{11} and P_{12}. Table 2 numbers the planes and shows which combination of points define each plane. Figure 7 shows the resulting planes as well as the resulting shape of the 3D-MFD for an artificial network. We consider this set as the minimal amount of planes required to describe the fundamental relationships in the 3D-MFD. It should be clear, however, that this set of thirteen points and the set of nine planes is not the ultimate and complete solution to describe

Plane	Points	Description
I	P_0, P_7, P_9	Free flow traffic conditions in both modes. The tilting of the plane describes the trade-off between cars and buses achieving the same travel production.
II	P_1, P_3, P_{10}	Backward wave speed for car only traffic.
III	P_5, P_6, P_9, P_{10}	Describes increase in travel production when car network is saturated and buses on their dedicated network add to the travel production.
IV	P_3, P_4, P_9	Wave speed of mixed traffic. The points P_6 is favored over P_{10} as traffic states might deteriorate faster due to mixed traffic conditions.
V	P_7, P_8, P_9	Capacity trade-off between buses and cars when the bus system operates in the saturated state.
VI	P_2, P_8, P_9	Capacity trade-off between buses and cars when the bus system operate sin the congested state.
VII	P_2, P_4, P_9	Capacity trade-off between buses and cars when both system operate in the saturated state. We extend this plane also to the congested state of buses to reduce the number of planes.
When describing mixed traffic operations		
VIII	P_8, P_{11}, P_{12}	Replaces the trade-off between buses and cars when both systems operate in free-flow conditions.
IX	P_3, P_4, P_{12}	Replaces the trade-off between buses and cars when both modes operate in congested states.

Table 2: Construction of the nine planes from the twelve points.

the 3D-MFD. Many more points can be defined to capture certain traffic characteristics; also more planes can be introduced as well and some planes can become non-binding. Further, we acknowledge that there are also other combinations of points for the proposed planes that lead to a similar 3D-MFD shape.

Plane I characterizes mixed traffic conditions when both modes operate in free flow conditions. The tilting of this plane represents the number of cars that can be replaced by a bus to achieve the same travel production. Plane II captures the traffic states when car traffic is in the congested state and given the location of this plane, bus operates in free flow conditions. Plane III describes the behavior in the network that when all roads where cars can circulate operate in the saturated state, running more buses on the dedicated bus network increases the total travel production. This contribution is usually rather small, but can become substantial in case of bus rapid transit systems and when it comes to passenger transportation. Plane IV models the

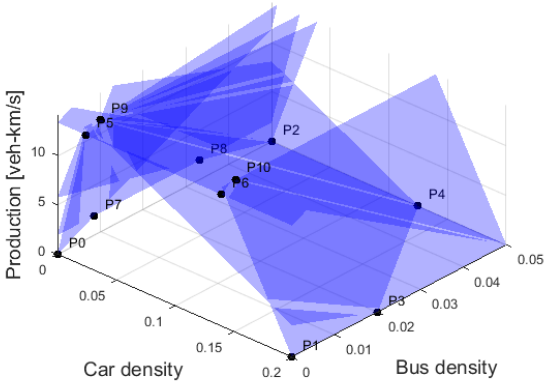

(a) Planes I-VII, view A

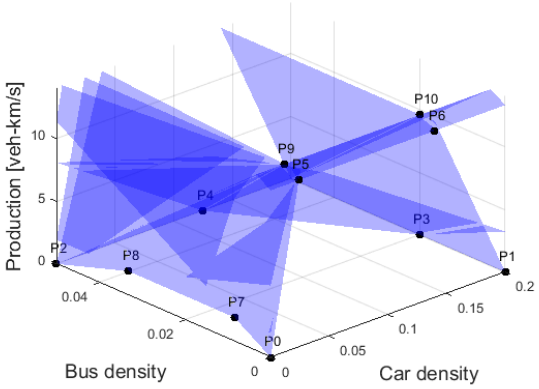

(b) Planes I-VII, view B

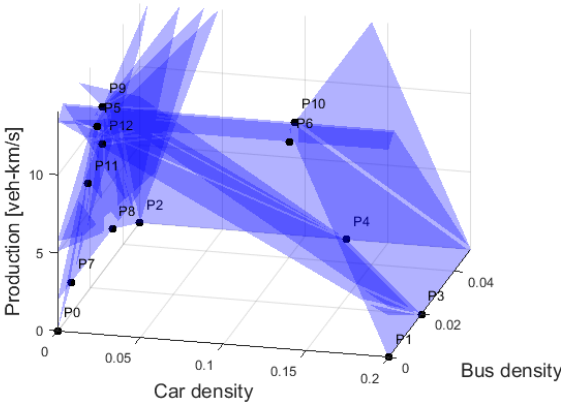

(c) Planes I-IX, view A

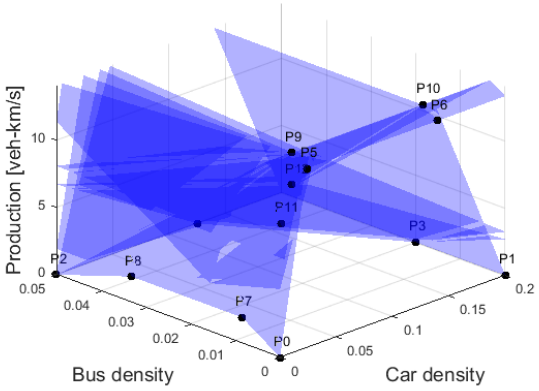

(d) Planes I-IX, view B

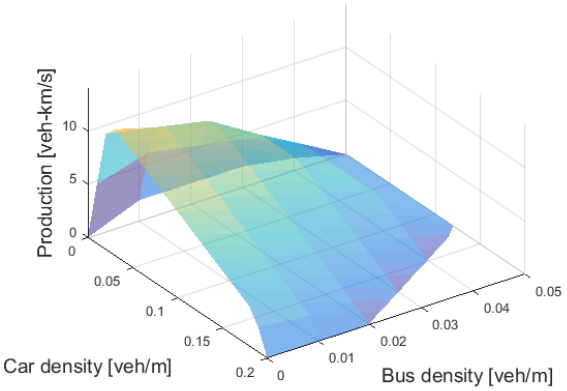

(e) 3D-MFD with planes I-VII, view A

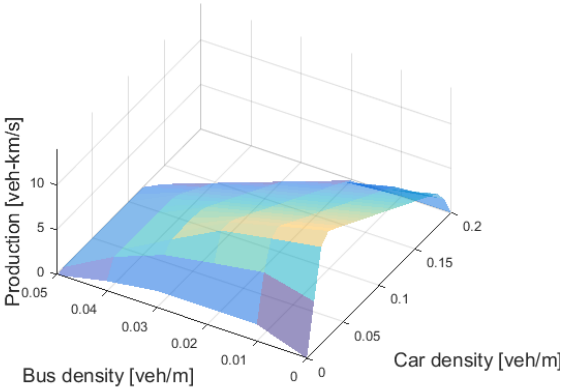

(f) 3D-MFD with planes I-VII, view B

Figure 7: Illustrating the planes and the resulting 3D-MFD

congested state in both modes and all sub networks. We propose to use P_6 instead of possibly more obvious P_{10} for two reasons. First, once the multi-modal system reaches its capacity we consider that the system in mixed traffic deteriorates faster to grid lock than if only cars would circulate. Second, with this approach we require less planes making the entire formulation of the 3D-MFD much simpler. Planes V and VI complement plane I with respect to saturated and congested operations in the bus network. Considering these planes might be more relevant to cities where bus lines at central hub locations are overlapping to a large extent, e.g. in Zurich or Brisbane. The last required plane is plane VII that closes the 3D-MFD and creates the familar shape. It describes the trade-off between buses and cars when both are operating in the saturated state, however, we propose to further include the congested state of bus network for two reasons. First, the traffic state at these locations in the 3D-MFD might be rarely required in applications. Second, we can reduce the number of planes and thus the complexity of the formulation.

The operational mixed traffic behavior described by P_{11} and P_{12} can be included in the 3D-MFD shape using planes VIII and IX. Plane VIII adds further information to the free flow part and thus affects all planes located in this area, while plane IX mostly affects planes II and IV. In Figure 7 we include in exhibits 7(c) and 7(d) the planes including P_{11} and P_{12}. One can clearly see how this operational feature reduces the overall multi-modal capacity of the system as well as slowing down car traffic.

In Figures 7(e) and 7(f) we then use the set of planes from Table 2 and Eqn. 5 to derive the functional form for the 3D-MFD and to obtain the familar shape as introduced by Geroliminis et al. (2014). For these forms we have chosen a small value of $\lambda = 0.1$ to ensure a tight fit of the curve to the shape defned by the planes. This small value then results in the somehow kinky shape of the 3D-MFD, but the larger λ is chosen the smoother the entire shape becomes.

We have to explicitly and clearly state that the definitions and assumptions for the points are optimistic and describe the highest possible travel production for any combination of bus and car accumulations. Although empirical observations will be by definition always below the defined curve of the 3D-MFD, the deviation can be substantial when the vehicle interactions (measured by λ) are rather strong and spatial heterogeneity is large. However, as Eqn. 5 is flexible to accommodate many more planes as proposed here, more realistic points and planes, especially for the bus operations, can be defined and included, which all then results in a more accurate 3D-MFD for the specific context. For example, the method of cuts by Daganzo and Geroliminis (2008) can further be used - if applicable - to derive more points and then planes to define in the end a more tighter 3D-MFD shape.

3 Applications of the functional form

We now discuss policy and traffic engineering relevant applications for the proposed functional form. We first describe in Section 3.1 the derivation of the 3D-MFD passenger MFD from a vehicle occupancy capacity perspective. Then in Section 3.2 from a passengers with preferences perspective. We then show how to obtain an estimate of the overall productivity of multi-modal urban road networks in Section 3.3.

3.1 The vehicle occupancy capacity 3D-MFD

For the derivation of the vehicle occupancy capacity 3D-MFD we follow the procedure proposed by Geroliminis et al. (2014). The passenger travel production Pax results, as shown in Eqn. 11, from the sum of the vehicle travel production times vehicle occupancy capacity. h_b is defined as bus occupancy and h_c as car occupancy.

$$Pax = N_b h_b v_{b,MFD} + N_c h_c v_{c,MFD} \tag{11}$$

Eqn. 11 requires that bus $v_{b,MFD}$ and car speeds $v_{c,MFD}$ are endogenously derived from the 3D-MFD. The endogenous speed of each mode cannot be directly derived from the 3D-MFD as the 3D-MFD only provides the average speed of the system with $v_{MFD} := \Pi / (N_c + N_b)$. Thus, to solve for each mode's commercial speed we require another constraint. Geroliminis et al. (2014) propose to use an linear relationship between both modes speeds as provided in the right hand side of Eqn. 12 with intercept β and slope θ. For our analysis, we propose the linear relationship on the left hand side of Eqn. 12 from the following two cases. First, in light traffic cars drive at $v_{c,MFD} = v_c$ and buses are not obstructed by cars and run at $v_{b,MFD} = v_b$. Second, when the entire car network is gridlocked, the speed of cars is $v_{c,MFD} = 0$and buses only run on their dedicated lanes with v_b. Assuming that buses are equidistantly spaced on their lines, the average space mean speed of buses is the fraction of dedicated bus lanes to the entire bus network. Then the speeds of each mode can be coupled as Eqn. 12. The values for β and θ can be read from Eqn. 12. Nevertheless, we consider Eqn. 12 only holding approximately and not over the entire range of vehicle accumulations. Therefore, we further require that for each mode, the speed is always within the fundamental diagram of that mode as shown in Eqn. 1. Additionally for the bus speed, we define that the speed equals the MFD speed when the car network is jammed, i.e. car speed is zero, to avoid negative bus speeds. Then, each mode's

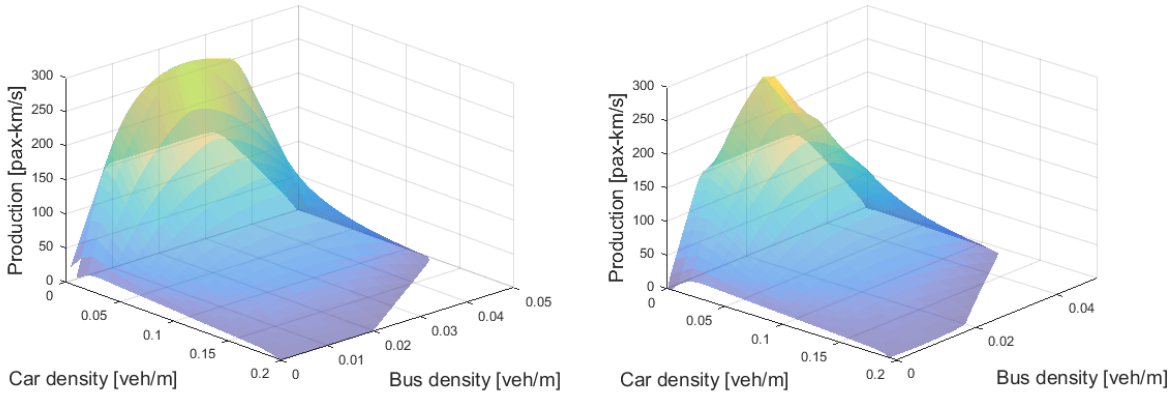

(a) 3D-MFD for vehicle occupancy capacity based on 3D-MFD average speed

(b) 3D-MFD for vehicle occupancy capacity based on mode average speed

Figure 8: Comparing vehicle occupancy capacity 3D-MFDs. Car occupancy is assumed to be equal to two, while bus occupancy is assumed to be 80. The underlying 3D-MFD is identical to those shown in Figure 7.

speed is given by Eqn. 13 for cars and 14 for buses, respectively.

$$v_{b,MFD} = \underbrace{v_b \frac{\eta_b}{1-\eta_c}}_{\beta} + \underbrace{v_b \frac{(1-\eta_b/(1-\eta_c))}{v_c}}_{\theta} v_{c,MFD} \tag{12}$$

$$v_{c,MFD} = \min\left(\frac{\min\left(v_c k_c; s(G/C); w_c\left(\kappa_c - k_c\right)\right)}{k_b}; \frac{\Pi - \beta N_b}{N_c + \theta N_b}\right) \tag{13}$$

$$v_{b,MFD} = \min\left(\frac{\min\left(v_b k_b; s_{bus}\left(\frac{p/\bar{v}_b}{p/\bar{v}_b + \Delta}\right)\left(1 + \left(\frac{G}{C} - 1\right)\zeta\right); w_b\left(\kappa_b - k_b\right)\right)}{k_b}; \frac{\Pi - \beta N_b}{N_c + \theta N_b}\theta + \beta; v_{MFD}\right) \tag{14}$$

In Figure 8 we provide an example for a vehicle occupancy capacity 3D-MFD which is based on the 3D-MFD shown in Figure 7. We assume an average occupancy of vehicles as 2 for cars and 80 for buses. The vehicle occupancy capacity 3D-MFD shows clearly a maximum at non zero density of buses.

3.2 The passenger-preference 3D-MFD

We can use human preferences for mode choice and the information on vehicle interactions in the 3D-MFD to derive a passenger-preference 3D-MFD. Consider a population of N individuals, all of which choose their mode of transportation based on random utility maximization theory. Each individual has an underlying utility function U for each alternative, where the attributes of each alternative define the level of utility. The alternative with highest utility is then chosen. Attributes are typically travel time and cost, the headway, distance to the next bus stop, vehicle crowding etc. For simplicity, we assume that preferences are identical across the population as are the attribute levels for each alternative in the network. Further, as the choice between car and bus is discrete, and we prefer an expression on probabilities of choice instead of utility levels, we choose the *logit* model for linking the utility levels to probabilities (McFadden, 1974).

Thus, to derive the number of bus travellers N_{bus} from the entire population N we use Eqn. 15 where the attribute levels of each alternative are stored in vector $\boldsymbol{x}$ while its valuation in terms of utility is stored in vector $\boldsymbol{\beta}$.

$$N_{bus} = \frac{N}{1 + \exp\left(-\boldsymbol{x}^T \boldsymbol{\beta}\right)} \tag{15}$$

In the current 3D-MFD parametrization, we only use the number of buses, but public transport agencies as well as travellers make their decision not based on N_b, but based on the design variables of the public transport system. The work by Daganzo (2010) allows us to link the 3D-MFD to the stop spacing p, headway h, network design α and commercial speed v_b. Eqn. 16 describes how the network design parameter α is calculated and Eqn. 17 how all parameters are linked to each other.

$$\alpha = \sqrt{\left(1 - \eta_c\right) \frac{pL}{D^2} - 1} \tag{16}$$

$$h = \frac{2D^2}{pN_b v_b} \left(3\alpha - \alpha^2\right) \tag{17}$$

In this analysis, we discuss how the total number of travellers and the design headway in the

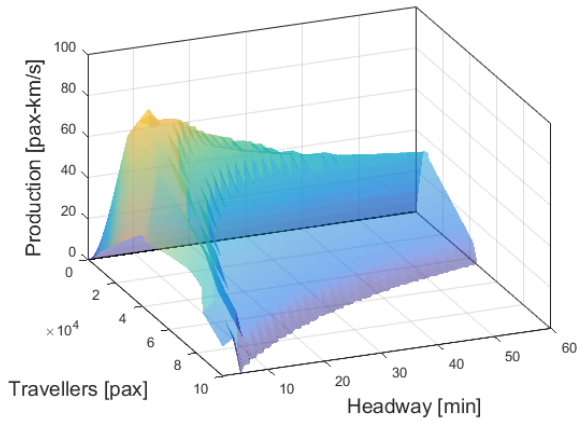

Figure 9: The passenger preference 3D-MFD in the dimensions of total number of travellers and design headway of the system.

network is linked to the travel production when individuals choose their mode. For $\boldsymbol{\beta}$ in Eqn. 15 we select typical values for headway, walking time to the next stop, travel time for a 6 km trip and one transfer. Figure 9 shows the results based on the 3D-MFD shown in Figure 7. The 3D-MFD clearly shows that reducing the headway increases the total number of people that can be transported as more choose the bus instead of the car. This then further increases the total trip production.

3.3 Productivity of urban road networks

The policy related question *How many cars are too many?* can now be easily answered with the 3D-MFD and our proposed link to the allocation of urban resources. This approach allows to identify the limit to the number of people that can be transported with the available infrastructure. Figure 10 relates the total number of travellers and the mode share to the total travel production based on the 3D-MFD introduced in Figure 7. We observe a distinct exponential curve between moving traffic states and grid lock, a similar relationship is observed for the maximum trip production.

Now, with this approach cities and transport authorities are enabled to estimate the productivity of their networks given certain resources without running simulation after simulation.

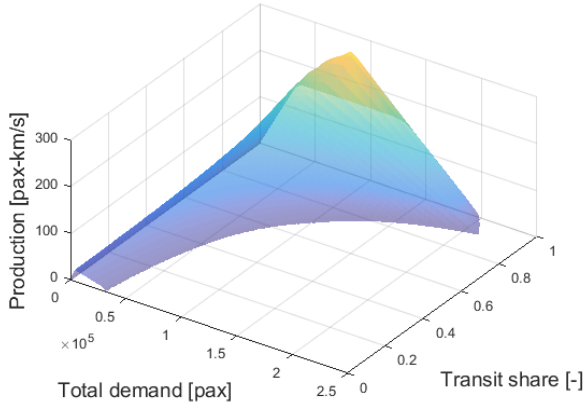

Figure 10: Analyzing the productivity of urban networks with the 3D-MFD.

4 Empirical 3D-MFDs

In this section, we apply Eqn. 5 together with planes I-XI to two empirical data sets. We collected car traffic data from inductive loop detectors in London and in Zurich that provide vehicle flows and occupancy. Figures 11(a) and 11(b) show the experimental site. For the bus data, we collected data from the automated vehicle location devices (AVL) that allows to reconstruct the trajectories of vehicles and as such the estimation of the averages of speed and density. The data from Zurich has been previously used by Loder et al. (2017). From the data sets as well as network topology obtained from OpenStreetMap, we derived the parameters listed in Table 3.

For London and for Zurich in Figures 11(c) to 11(f) we perhaps surprisingly observe that the empirical points align smoothly with the proposed shape and that the observed maximum further is close to the maximum suggested by the 3D-MFD. In both cases, we observe parts of a well-defined congested branch for car traffic, while the variation in buses is not that large. However, for London in Figures 11(c) and 11(d) we observe a slightly larger variation than for Zurich in Figures 11(e) and 11(f). This can be explained that the network exhibit from Zurich is smaller and thus more homogeneous in terms of public transport operations with a rather rigid time table with headways always between 7.5 and 10 minutes.

The comparison between the empirical points with the proposed 3D-MFD functional form emphasizes that in empirical contexts the full range of densities are not observed as it can be for simulation data (Geroliminis et al., 2014). This further finding makes it rather difficult to apply the functional form proposed by the previously named authors when no simulation data is available, while this is still possible with our proposed functional form.

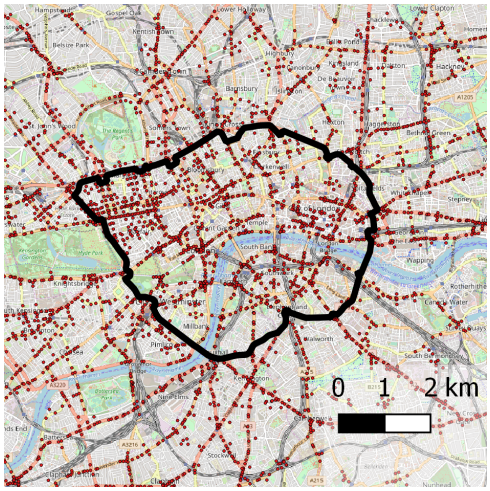

(a) Region of analysis in London (UK)

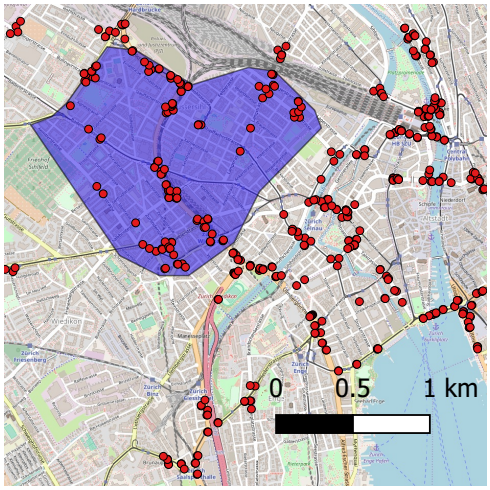

(b) Region of analysis in Zurich (CH)

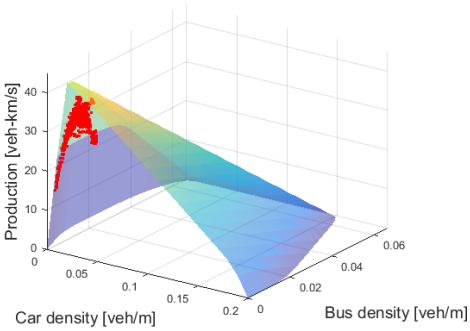

(c) 3D-MFD of London, view A

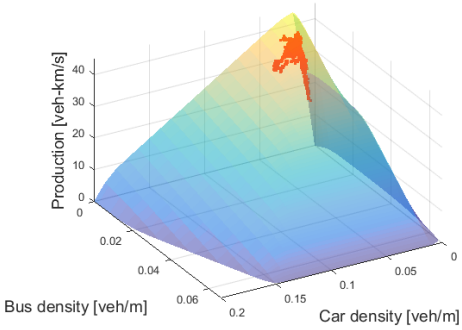

(d) 3D-MFD of London, view B

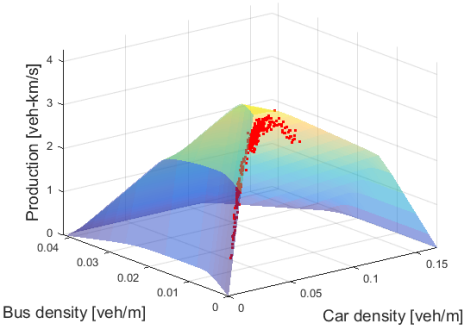

(e) 3D-MFD of Zurich, view A

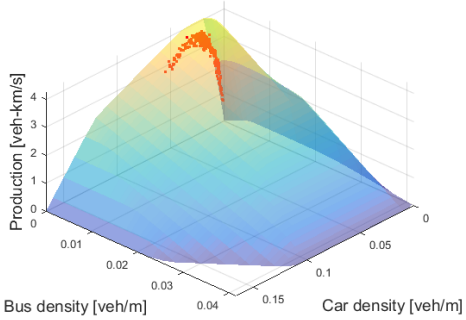

(f) 3D-MFD of Zurich, view B

Figure 11: Comparing the empirical 3D-MFDs with the proposed functional form for a neighborhood in London and Zurich.

Parameter	London	Zurich
Network length	354	46
Dedicated bus network	0.08	0.32
Dedicated car network	0.69	0.46
Car length	0.005	0.006
Bus-car length ratio	3	4
Free flow speed cars (including intersection delay)	28	27
Wave speed cars (including intersection delay)	6	6
Free flow speed buses (w/o intersection delay)	21	22
Wave speed buses	5	5
Saturation flow	1600	1600
Average block length	0.23	0.28
Average stop spacing	0.33	0.35
Cycle length	62	55
Effective green time	19	16
Average dwell-time	18	28
ζ	0.4	0.1
δ_c	0.006	0.006
λ	1	0.05

Table 3: Caption

5 Conclusions

This paper proposes a new functional form for the 3D-MFD for modeling the multi-modal operations of urban traffic, where the interactions between vehicles are quantified by just a single parameter. The shape defining parameters of the functional form are derived from the physical and operational characteristics of the multi-modal urban networks. The functional form is flexible to accommodate further city-specific characteristics in the traffic operations such as taxi and mini bus operations.

The 3D-MFD and this proposed functional form offer applications a system perspective where transport is only considered as a trip producing factory where no time consuming network assignment is necessary anymore. Planners and engineers can use our proposed functional form for the 3D-MFD to analyze changes in the urban resource allocation on the overall productivity of urban road networks. By doing so, this approach allows a rather quick determination whether a city is *full* and demands other means of transportation such as an underground.

This macroscopic approach of multi-modal urban transportation describe interactions under steady-state conditions, but lacks microscopic detail and is not capable of considering dynamic aspects of urban traffic. Future research needs to investigate this. Further, the analytical approaches to the MFD (Daganzo and Geroliminis, 2008; Leclercq and Geroliminis, 2013) and bus operations (Daganzo, 2010; Eichler and Daganzo, 2006) should be more tightly bound to this functional form to improve the shape of the functional form.

The discussed applications of the functional form for the 3D-MFD emphasize the practical and policy relevant implications of this research. First, it allows to understand multi-modal urban traffic even with only low data requirements. Second, this approach provides the first mean to analyze analytically the question *how many cars are too many?* and provide a simple tool to understand the relationship between urban resources and productivity.

Acknowledgement

This work was supported by ETH Research Grants ETH-04 15-1 and ETH-27 16-1. We wish to acknowledge the support by Ashley Turner and Andy Emmonds from London, and Gian Dönier, Urs Birchmeier and Karl Weberruss from Zurich.

6 References

Ambühl, L., A. Loder, M. Bliemer, M. Menendez and K. W. Axhausen (2017) A functional form for the macroscopic fundamental diagram with a physical meaning, *Arbeitsberichte Verkehrs- und Raumplanung*, **1306**.

Boyaci, B. and N. Geroliminis (2011) Estimation of the network capacity for multimodal urban systems, *Procedia - Social and Behavioral Sciences*, **16**, 803–813.

Castrillon, F. and J. Laval (2017) Impact of buses on the macroscopic fundamental diagram of homogeneous arterial corridors, *Transportmetrica B: Transport Dynamics*, **in press**, 1–16.

Chiabaut, N. (2015) Evaluation of a multimodal urban arterial: The passenger macroscopic fundamental diagram, *Transportation Research Part B: Methodological*, **81, Part 2**, 410–420.

Daganzo, C. F. (2007) Urban gridlock: Macroscopic modeling and mitigation approaches, *Transportation Research Part B: Methodological*, **41**, 49–62.

Daganzo, C. F. (2010) Structure of competitive transit networks, *Transportation Research Part B: Methodological*, **44** (4) 434–446.

Daganzo, C. F. and N. Geroliminis (2008) An analytical approximation for the macroscopic fundamental diagram of urban traffic, *Transportation Research Part B: Methodological*, **42**, 771–781.

Daganzo, C. F. and L. J. Lehe (2016) Traffic flow on signalized streets, *Transportation Research Part B*, **90**, 56–69.

Daganzo, C. F., L. J. Lehe and J. Argote-Cabanero (2017) Adaptive offsets for signalized streets, *Transportation Research Part B: Methodological*, 1–9.

Eichler, M. and C. F. Daganzo (2006) Bus lanes with intermittent priority: Strategy formulae and an evaluation, *Transportation Research Part B: Methodological*, **40** (9) 731–744.

Geroliminis, N., N. Zheng and K. Ampountolas (2014) A three-dimensional macroscopic fundamental diagram for mixed bi-modal urban networks, *Transportation Research Part C: Emerging Technologies*, **42**, 168–181.

Guler, S. I. and M. Menendez (2014) Analytical formulation and empirical evaluation of pre-signals for bus priority, *Transportation Research Part B: Methodological*, **64**, 41–53.

Leclercq, L. and N. Geroliminis (2013) Estimating mfds in simple networks with route choice, *Transportation Research Part B: Methodological*, **57**, 468–484.

Loder, A., L. Ambühl, M. Menendez and K. W. Axhausen (2017) Empirics of multi-modal traffic networks - using the 3d macroscopic fundamental diagram, *Transportation Research Part C: Emerging Technologies*, **82**, 88–101.

McFadden, D. (1974) Conditional logit analysis of qualitative choice behavior, *Frontiers in Econometrics*, 105–142.

Nagai, R., T. Nagatani and N. Taniguchi (2005) Traffic states and jamming transitions induced by a bus in two-lane traffic flow, *Physica A: Statistical Mechanics and its Applications*, **350** (2-4) 548–562.

Smeed, R. J. (1968) Traffic studies and urban congestion, *Journal of Transport Economics and Policy*, **2**, 33–70.